Generalized Hanbury Brown–Twiss effect and Stokes scintillations in the focal plane of a lens

Yangyundou Wang
School of Marine Science and Technology, Northwestern Polytechnical University, Xi'an, Shaanxi 710072, China
and Wellman Center for Photomedicine, Massachusetts General Hospital, Harvard Medical School, Boston, Massachusetts 02114, USA

Shenggang Yan
School of Marine Science and Technology, Northwestern Polytechnical University, Xi'an, Shaanxi 710072, China

David Kuebel
Department of Physics and Astronomy, University of Rochester, Rochester, New York 14627, USA
and Department of Physics, St. John Fisher College, Rochester, New York 14618, USA

Taco D. Visser
Department of Physics and Astronomy, Vrije Universiteit Amsterdam, 1081 HV Amsterdam, Netherlands
and Department of Physics and Astronomy, University of Rochester, Rochester, New York 14627, USA

(Received 14 March 2019; published 14 August 2019)

We explore the recently introduced concept of a generalized Hanbury Brown–Twiss (HBT) effect as applied to the focal plane of a lens that is used to focus a random electromagnetic beam. We find that the strength of the HBT correlation can be increased by the lens. Furthermore, the associated Stokes scintillations of the focused field display a surprisingly complicated spatial behavior. We illustrate, using the sum rules for scintillations and correlations, how focused fields can be tuned for different applications.

DOI: 10.1103/PhysRevA.100.023821

I. INTRODUCTION

The Hanbury Brown–Twiss (HBT) effect, named after its two discoverers, was originally applied to astronomy [1–3]. From the observed correlation of the intensity fluctuations at two detectors the angular size of radio stars could be determined. The original application assumed scalar fields originating from distant sources. Since then, other researchers have extended the HBT effect to vector fields and to observation points that are not necessarily in the far zone [4–13]. Recently, a polarization-resolved version of the HBT effect was studied in [14]. There it was found that the effect is just one manifestation of many possible correlations of fluctuations of the four Stokes parameters. In a similar vein, the concept of scintillation was also extended using the more general notion of Stokes fluctuations. This framework has since been used to study these correlations in random electromagnetic beams [15].

The classical treatment of the focusing of light assumes a deterministic wave field [16]. However, when the field is random, the intensity distribution [17,18], the state of coherence [19,20], and the degree of polarization [21] in the focal region are strongly affected. Moreover, the Stokes parameters, which describe the state of polarization of the focused field, then become stochastic quantities. The first Stokes parameter, denoted by S_0, describes the total intensity. That means that the correlation of the fluctuations of S_0 are identical to the HBT effect. Likewise, the variance of S_0 is equivalent to the scintillation of the field. Extending the notion of fluctuation correlations and variances to all four Stokes parameters, as was done in [14], has led to the insight that (a) these correlations can all be described by a single formula and (b) the correlations and scintillations are not independent, but rather satisfy certain sum rules. In this study we consider the HBT effect and the scintillation, together with their generalized versions, for the case of a random electromagnetic beam that is focused by a thin paraxial lens. We find that the distribution of the Stokes scintillations has a complicated structure and show that whereas the HBT correlation can be increased by the lens, the other Stokes fluctuation correlations can be decreased. Also, it is illustrated how the sum rules can be applied to design focused fields in which certain scintillations or correlations are suppressed.

II. STOKES PARAMETERS AND THEIR FLUCTUATIONS

The state of polarization of an electromagnetic beam at position $\mathbf{r}$ and at frequency ω can be characterized by the four spectral Stokes parameters, denoted by $S_n(\mathbf{r}, \omega)$, with $n = 0, 1, 2, 3$. A more complete characterization of such a beam, which also describes its two-point coherence properties, is provided by the cross-spectral density matrix, which is defined as [22]

$$\boldsymbol{W}(\mathbf{r}_1, \mathbf{r}_2, \omega) = \begin{pmatrix} W_{xx} & W_{xy} \\ W_{yx} & W_{yy} \end{pmatrix}, \tag{1}$$

where all the matrix elements are functions of the same three variables and are given by the expression

$$W_{ij}(\mathbf{r}_1, \mathbf{r}_2, \omega) = \langle E_i^*(\mathbf{r}_1, \omega) E_j(\mathbf{r}_2, \omega) \rangle \quad (i, j = x, y). \tag{2}$$

The angular brackets indicate an average taken over an ensemble of beam realizations. The expectation value of the Stokes parameters can be expressed in terms of the cross-spectral density matrix, evaluated at coincident points, as follows [22]:

$$\langle S_0(\mathbf{r},\omega)\rangle = W_{xx}(\mathbf{r},\mathbf{r},\omega) + W_{yy}(\mathbf{r},\mathbf{r},\omega), \tag{3a}$$

$$\langle S_1(\mathbf{r},\omega)\rangle = W_{xx}(\mathbf{r},\mathbf{r},\omega) - W_{yy}(\mathbf{r},\mathbf{r},\omega), \tag{3b}$$

$$\langle S_2(\mathbf{r},\omega)\rangle = W_{xy}(\mathbf{r},\mathbf{r},\omega) + W_{yx}(\mathbf{r},\mathbf{r},\omega), \tag{3c}$$

$$\langle S_3(\mathbf{r},\omega)\rangle = i[W_{yx}(\mathbf{r},\mathbf{r},\omega) - W_{xy}(\mathbf{r},\mathbf{r},\omega)]. \tag{3d}$$

The fluctuation of each Stokes parameter around its average value is defined as

$$\Delta S_n(\mathbf{r},\omega) = S_n(\mathbf{r},\omega) - \langle S_n(\mathbf{r},\omega)\rangle \quad (n=0,1,2,3), \tag{4}$$

where $S_n(\mathbf{r},\omega)$ is the spectral Stokes parameter pertaining to a single realization of the beam. The 4×4 matrix $\mathbf{C}(\mathbf{r}_1,\mathbf{r}_2,\omega)$, which describes all possible pairs of correlations between the various Stokes fluctuations, is defined as [14]

$$C_{nm}(\mathbf{r}_1,\mathbf{r}_2,\omega) \equiv \langle \Delta S_n(\mathbf{r}_1,\omega)\Delta S_m(\mathbf{r}_2,\omega)\rangle \quad \text{with } (n,m=0,1,2,3). \tag{5}$$

Under the assumption that the source that generates the beam is governed by Gaussian statistics, the 16 elements of this Stokes fluctuation correlation matrix can be expressed in terms of the cross-spectral density matrix as

$$C_{nm}(\mathbf{r}_1,\mathbf{r}_2,\omega) = \sum_{ab}\sum_{cd} \sigma_{ab}^n \sigma_{cd}^m W_{ad}(\mathbf{r}_1,\mathbf{r}_2,\omega) W_{bc}^*(\mathbf{r}_1,\mathbf{r}_2,\omega) \quad \text{with } (a,b,c,d=x,y), \tag{6}$$

where $\boldsymbol{\sigma}^0$ denotes the 2×2 identity matrix and the three Pauli spin matrices are defined as

$$\boldsymbol{\sigma}^1 = \begin{pmatrix} 1 & 0 \\ 0 & -1 \end{pmatrix}, \quad \boldsymbol{\sigma}^2 = \begin{pmatrix} 0 & 1 \\ 1 & 0 \end{pmatrix}, \quad \boldsymbol{\sigma}^3 = \begin{pmatrix} 0 & -i \\ i & 0 \end{pmatrix}. \tag{7}$$

For example, we find for the element C_{23} that

$$C_{23}(\mathbf{r}_1,\mathbf{r}_2) = \sum_{ab}\sum_{cd} \sigma_{ab}^2 \sigma_{cd}^3 W_{ad}(\mathbf{r}_1,\mathbf{r}_2) W_{bc}^*(\mathbf{r}_1,\mathbf{r}_2) \tag{8}$$

$$= i[W_{xx}(\mathbf{r}_1,\mathbf{r}_2)W_{yy}^*(\mathbf{r}_1,\mathbf{r}_2) + W_{yx}(\mathbf{r}_1,\mathbf{r}_2)W_{xy}^*(\mathbf{r}_1,\mathbf{r}_2)] - i[W_{xx}^*(\mathbf{r}_1,\mathbf{r}_2)W_{yy}(\mathbf{r}_1,\mathbf{r}_2) + W_{yx}^*(\mathbf{r}_1,\mathbf{r}_2)W_{xy}(\mathbf{r}_1,\mathbf{r}_2)] \tag{9}$$

$$= -2\,\mathrm{Im}[W_{xx}(\mathbf{r}_1,\mathbf{r}_2)W_{yy}^*(\mathbf{r}_1,\mathbf{r}_2) + W_{yx}(\mathbf{r}_1,\mathbf{r}_2)W_{xy}^*(\mathbf{r}_1,\mathbf{r}_2)] \tag{10}$$

$$= 2\,\mathrm{Im}[W_{xx}^*(\mathbf{r}_1,\mathbf{r}_2)W_{yy}(\mathbf{r}_1,\mathbf{r}_2) + W_{xy}(\mathbf{r}_1,\mathbf{r}_2)W_{yx}^*(\mathbf{r}_1,\mathbf{r}_2)], \tag{11}$$

where for brevity the ω dependence of the various quantities has been suppressed. Likewise, it is derived from Eq. (6) that the HBT coefficient, which describes the correlation of the total intensity fluctuation ΔS_0 at two points, is given by the expression

$$C_{00}(\mathbf{r}_1,\mathbf{r}_2) = |W_{xx}(\mathbf{r}_1,\mathbf{r}_2)|^2 + |W_{xy}(\mathbf{r}_1,\mathbf{r}_2)|^2 + |W_{yx}(\mathbf{r}_1,\mathbf{r}_2)|^2 + |W_{yy}(\mathbf{r}_1,\mathbf{r}_2)|^2. \tag{12}$$

Because of the nature of the Pauli spin matrices, all elements of the **C** matrix consist of a sum of four, rather than 16, terms. We emphasize that while the correlations of the fluctuations of the Stokes parameters are given by Eq. (6), the Stokes parameters themselves are related by the inequality [22]

$$\langle S_1(\mathbf{r})\rangle^2 + \langle S_2(\mathbf{r})\rangle^2 + \langle S_3(\mathbf{r})\rangle^2 \leqslant \langle S_0(\mathbf{r})\rangle^2. \tag{13}$$

The equal sign holds only for the case of a fully polarized beam.

When the two spatial arguments of the **C** matrix coincide, it reduces to the Stokes scintillation matrix **D**, i.e.,

$$D_{nm}(\mathbf{r}) \equiv C_{nm}(\mathbf{r},\mathbf{r}). \tag{14}$$

It is useful to introduce a normalized version of the **C** and the **D** matrices, both indicated by the superscript N, by defining

$$C_{nm}^N(\mathbf{r}_1,\mathbf{r}_2) = \frac{C_{nm}(\mathbf{r}_1,\mathbf{r}_2)}{\langle S_0(\mathbf{r}_1)\rangle\langle S_0(\mathbf{r}_2)\rangle}, \tag{15}$$

$$D_{nm}^N(\mathbf{r}) = \frac{D_{nm}(\mathbf{r})}{\langle S_0(\mathbf{r})\rangle^2}. \tag{16}$$

It was shown in [14] that the trace of the normalized **C** matrix has a clear physical meaning, namely,

$$\sum_{n=0}^{3} C_{nn}^N(\mathbf{r}_1,\mathbf{r}_2) = 2|\eta(\mathbf{r}_1,\mathbf{r}_2)|^2. \tag{17}$$

In Eq. (17) the quantity $\eta(\mathbf{r}_1,\mathbf{r}_2)$ denotes the spectral degree of coherence, which is defined as [22]

$$\eta(\mathbf{r}_1,\mathbf{r}_2) = \frac{\mathrm{Tr}\,\mathbf{W}(\mathbf{r}_1,\mathbf{r}_2)}{\sqrt{\mathrm{Tr}\,\mathbf{W}(\mathbf{r}_1,\mathbf{r}_1)\mathrm{Tr}\,\mathbf{W}(\mathbf{r}_2,\mathbf{r}_2)}}. \tag{18}$$

(Note that this definition of the spectral degree of coherence differs from the one presented in [12]). The modulus of $\eta(\mathbf{r}_1,\mathbf{r}_2)$ is related to the visibility of the interference fringes in Young's experiment with the two pinholes located at $\mathbf{r}_1$ and $\mathbf{r}_2$. Since $\eta(\mathbf{r},\mathbf{r}) = 1$, it follows immediately that the diagonal elements of the normalized **D** matrix are not independent but are related by the sum rule

$$\sum_{n=0}^{3} D_{nn}^N(\mathbf{r}) = 2. \tag{19}$$

The first diagonal element $D_{00}^N(\mathbf{r})$ is the usual scintillation coefficient or, equivalently, the square of the scintillation index [23]. Under the assumption of Gaussian statistics, its bounds are [24]

$$\tfrac{1}{2} \leqslant D_{00}^N(\mathbf{r}) \leqslant 1. \tag{20}$$

Bounds for C_{00}^N were discussed in [13].

We note that both the Stokes fluctuations and the Stokes scintillations can be measured using a narrow-band spectral filter together with a division-of-amplitude photopolarimeter (see, for example, [25] and the references therein).

III. FOCUSING GAUSSIAN SCHELL-MODEL BEAMS

It is well known that a thin converging paraxial lens acts like a Fourier transformer for scalar fields. To be more precise, the field in the back focal plane is proportional to the Fourier transform of the field in the front focal plane [26]. A similar relation holds for the elements of the cross-spectral density matrix of an electromagnetic beam that is focused by such a

lens [27], i.e.,

$$W_{ij}^{(f)}(\boldsymbol{\rho}_1, \boldsymbol{\rho}_2) = \frac{1}{\lambda^2 f^2}\, \tilde{W}_{ij}^{(\mathrm{in})}(-k\boldsymbol{\rho}_1/f, k\boldsymbol{\rho}_2/f) \quad (i, j = x, y). \tag{21}$$

Here the superscripts (in) and (f) indicate the front focal plane and the back focal plane, respectively, and the vectors $\boldsymbol{\rho} = (x, y)$ describe a position in a plane that is transverse to the central axis, which is taken to be the z axis. Furthermore, the wave number $k = 2\pi/\lambda$, with λ the free-space wavelength, and f denotes the focal length. The spatial four-dimensional Fourier transform is defined as

$$\tilde{W}_{ij}^{(\mathrm{in})}(\mathbf{p}, \mathbf{q}) = \iint_{-\infty}^{\infty} W_{ij}^{(\mathrm{in})}(\boldsymbol{\rho}', \boldsymbol{\rho}'') \exp[-i(\mathbf{p}\cdot\boldsymbol{\rho}' + \mathbf{q}\cdot\boldsymbol{\rho}'')] d^2\rho' d^2\rho''. \tag{22}$$

Recently, Eq. (21) has been used to examine the effect of focusing on the degree of polarization [21,27]. Here we will apply it to the case of a partially coherent Gaussian Schell-model (GSM) beam and study the fluctuations of the various Stokes parameters and their correlations in the back focal plane of a thin paraxial lens. We assume that a source that generates a GSM beam is located in the front focal plane of the lens. The elements of the cross-spectral density matrix, which was introduced in Eq. (1), are then given by the expression [22]

$$W_{ij}^{(\mathrm{in})}(\boldsymbol{\rho}', \boldsymbol{\rho}'') = A_i A_j B_{ij} \exp\left[-\left(\frac{\rho'^2}{4\sigma_i^2} + \frac{\rho''^2}{4\sigma_j^2}\right)\right] \times \exp\left[-\frac{(\boldsymbol{\rho}'' - \boldsymbol{\rho}')^2}{2\delta_{ij}^2}\right]. \tag{23}$$

Here A_i denotes the spectral amplitude of E_i and B_{ij} describes the correlation of E_i and E_j. The symbols σ_i and δ_{ij} represent effective spatial widths and coherence radii, respectively. The parameters have to satisfy several constraints, i.e.,

$$B_{xx} = B_{yy} = 1, \tag{24}$$

$$B_{xy} = B_{yx}^*, \tag{25}$$

$$B_{xy} = |B_{xy}| e^{i\phi} \quad \text{where } |B_{xy}| \leqslant 1,\ \phi \in \mathbb{R}, \tag{26}$$

$$\delta_{xy} = \delta_{yx}. \tag{27}$$

Furthermore, the so-called realizability conditions are [28]

$$\sqrt{\frac{\delta_{xx}^2 + \delta_{yy}^2}{2}} \leqslant \delta_{xy} \leqslant \sqrt{\frac{\delta_{xx}\delta_{yy}}{|B_{xy}|}}. \tag{28}$$

This expression implies an upper bound for the modulus of B_{xy}, namely,

$$|B_{xy}| \leqslant \frac{2}{\delta_{xx}/\delta_{yy} + \delta_{yy}/\delta_{xx}}. \tag{29}$$

We restrict ourselves to the case that the two effective widths are identical, i.e., $\sigma_x = \sigma_y = \sigma$. Then the source will generate a beamlike field if [29]

$$\frac{1}{4\sigma^2} + \frac{1}{\delta_{xx}^2} \ll \frac{2\pi^2}{\lambda^2}, \quad \frac{1}{4\sigma^2} + \frac{1}{\delta_{yy}^2} \ll \frac{2\pi^2}{\lambda^2}. \tag{30}$$

On changing to sum and difference variables

$$\mathbf{R}_+ = \frac{\boldsymbol{\rho}' + \boldsymbol{\rho}''}{2}, \tag{31}$$

$$\mathbf{R}_- = \boldsymbol{\rho}'' - \boldsymbol{\rho}', \tag{32}$$

we find that the spatial Fourier transform of the cross-spectral density matrix (23) is given by the expression

$$\begin{aligned}\tilde{W}_{ij}^{(\mathrm{in})}(\mathbf{p}, \mathbf{q}) &= A_i A_j B_{ij} \int_{-\infty}^{\infty} \exp[-R_+^2/2\sigma^2] \exp[-i\mathbf{R}_+ \cdot (\mathbf{q} + \mathbf{p})] d^2R_+ \int_{-\infty}^{\infty} \exp\left[-R_-^2/2\Omega_{ij}^2\right] \exp[-i\mathbf{R}_- \cdot (\mathbf{q} - \mathbf{p})/2] d^2R_- \\ &= 4\pi^2 A_i A_j B_{ij} \sigma^2 \Omega_{ij}^2 \exp[-\sigma^2(\mathbf{q} + \mathbf{p})^2/2] \exp\left[-\Omega_{ij}^2(\mathbf{q} - \mathbf{p})^2/8\right],\end{aligned} \tag{33}$$

where

$$\frac{1}{\Omega_{ij}^2} = \frac{1}{\delta_{ij}^2} + \frac{1}{4\sigma^2}. \tag{34}$$

On substituting this into Eq. (21) we find that

$$W_{ij}^{(f)}(\boldsymbol{\rho}_1, \boldsymbol{\rho}_2) = \frac{4\pi^2 A_i A_j B_{ij} \sigma^2 \Omega_{ij}^2}{\lambda^2 f^2} \exp\left[-\frac{\sigma^2 k^2}{2f^2}(\boldsymbol{\rho}_2 - \boldsymbol{\rho}_1)^2\right] \times \exp\left[-\frac{\Omega_{ij}^2 k^2}{8f^2}(\boldsymbol{\rho}_1 + \boldsymbol{\rho}_2)^2\right]. \tag{35}$$

We will use this result in Eq. (6) to obtain expressions for the correlation of the Stokes fluctuations and the Stokes scintillations in the back focal plane.

IV. STOKES SCINTILLATIONS

For the four diagonal elements of the Stokes scintillation matrix we have from Eq. (6) and the definition (14) that

$$\begin{aligned} D_{00}(\boldsymbol{\rho}) &= |W_{xx}(\boldsymbol{\rho}, \boldsymbol{\rho})|^2 + |W_{xy}(\boldsymbol{\rho}, \boldsymbol{\rho})|^2 \\ &\quad + |W_{yx}(\boldsymbol{\rho}, \boldsymbol{\rho})|^2 + |W_{yy}(\boldsymbol{\rho}, \boldsymbol{\rho})|^2, \end{aligned} \tag{36a}$$

$$\begin{aligned} D_{11}(\boldsymbol{\rho}) &= |W_{xx}(\boldsymbol{\rho}, \boldsymbol{\rho})|^2 - |W_{xy}(\boldsymbol{\rho}, \boldsymbol{\rho})|^2 \\ &\quad - |W_{yx}(\boldsymbol{\rho}, \boldsymbol{\rho})|^2 + |W_{yy}(\boldsymbol{\rho}, \boldsymbol{\rho})|^2, \end{aligned} \tag{36b}$$

$$\begin{aligned} D_{22}(\boldsymbol{\rho}) &= 2\,\mathrm{Re}[W_{xx}(\boldsymbol{\rho}, \boldsymbol{\rho}) W_{yy}^*(\boldsymbol{\rho}, \boldsymbol{\rho}) \\ &\quad + W_{xy}(\boldsymbol{\rho}, \boldsymbol{\rho}) W_{yx}^*(\boldsymbol{\rho}, \boldsymbol{\rho})], \end{aligned} \tag{36c}$$

$$\begin{aligned} D_{33}(\boldsymbol{\rho}) &= 2\,\mathrm{Re}[W_{xx}(\boldsymbol{\rho}, \boldsymbol{\rho}) W_{yy}^*(\boldsymbol{\rho}, \boldsymbol{\rho}) \\ &\quad - W_{xy}(\boldsymbol{\rho}, \boldsymbol{\rho}) W_{yx}^*(\boldsymbol{\rho}, \boldsymbol{\rho})]. \end{aligned} \tag{36d}$$

On making use of Eq. (23) in these expressions, while setting $\sigma_x = \sigma_y = \sigma$, we find for the normalized Stokes scintillations in the front focal plane of the lens the formulas

$$D_{00}^{N(\mathrm{in})} = \frac{A_x^4 + A_y^4 + 2A_x^2A_y^2|B_{xy}|^2}{\left(A_x^2 + A_y^2\right)^2}, \tag{37a}$$

$$D_{11}^{N(\mathrm{in})} = \frac{A_x^4 + A_y^4 - 2A_x^2A_y^2|B_{xy}|^2}{\left(A_x^2 + A_y^2\right)^2}, \tag{37b}$$

$$D_{22}^{N(\mathrm{in})} = \frac{2A_x^2A_y^2[1 + |B_{xy}|^2\cos(2\phi)]}{\left(A_x^2 + A_y^2\right)^2}, \tag{37c}$$

$$D_{33}^{N(\mathrm{in})} = \frac{2A_x^2A_y^2[1 - |B_{xy}|^2\cos(2\phi)]}{\left(A_x^2 + A_y^2\right)^2}. \tag{37d}$$

We note that these four expressions are all uniform, i.e., the four Stokes scintillations are independent of the transverse position $\boldsymbol{\rho}$. It is easily verified that they obey the sum rule expressed by Eq. (19), namely,

$$\sum_{n=0}^{3} D_{nn}^{N(\mathrm{in})} = 2. \tag{38}$$

The Stokes scintillations in the back focal plane can be obtained by substituting from Eq. (35) into Eqs. (36a)–(36d). This gives

$$\begin{aligned} D_{00}^{N(f)}(\rho) = {} & \left[A_x^4\Omega_{xx}^4 \exp\left(-\Omega_{xx}^2k^2\rho^2/f^2\right) + A_y^4\Omega_{yy}^4\right. \\ & \times \exp\left(-\Omega_{yy}^2k^2\rho^2/f^2\right) + 2A_x^2A_y^2\Omega_{xy}^4|B_{xy}|^2 \\ & \left.\times \exp\left(-\Omega_{xy}^2k^2\rho^2/f^2\right)\right]/\Lambda^2(\rho), \end{aligned} \tag{39a}$$

$$\begin{aligned} D_{11}^{N(f)}(\rho) = {} & \left[A_x^4\Omega_{xx}^4 \exp\left(-\Omega_{xx}^2k^2\rho^2/f^2\right) + A_y^4\Omega_{yy}^4\right. \\ & \times \exp\left(-\Omega_{yy}^2k^2\rho^2/f^2\right) - 2A_x^2A_y^2\Omega_{xy}^4|B_{xy}|^2 \\ & \left.\times \exp\left(-\Omega_{xy}^2k^2\rho^2/f^2\right)\right]/\Lambda^2(\rho), \end{aligned} \tag{39b}$$

$$\begin{aligned} D_{22}^{N(f)}(\rho) = {} & 2A_x^2A_y^2\left\{\Omega_{xx}^2\Omega_{yy}^2 \exp\left[-\left(\Omega_{xx}^2 + \Omega_{yy}^2\right)k^2\rho^2/2f^2\right]\right. \\ & + \Omega_{xy}^4|B_{xy}|^2\cos(2\phi) \\ & \left.\times \exp\left(-\Omega_{xy}^2k^2\rho^2/f^2\right)\right\}/\Lambda^2(\rho), \end{aligned} \tag{39c}$$

$$\begin{aligned} D_{33}^{N(f)}(\rho) = {} & 2A_x^2A_y^2\left\{\Omega_{xx}^2\Omega_{yy}^2 \exp\left[-\left(\Omega_{xx}^2 + \Omega_{yy}^2\right)k^2\rho^2/2f^2\right]\right. \\ & - \Omega_{xy}^4|B_{xy}|^2\cos(2\phi) \\ & \left.\times \exp\left(-\Omega_{xy}^2k^2\rho^2/f^2\right)\right\}/\Lambda^2(\rho), \end{aligned} \tag{39d}$$

where

$$\begin{aligned} \Lambda(\rho) = {} & A_x^2\Omega_{xx}^2 \exp\left(-\Omega_{xx}^2k^2\rho^2/2f^2\right) \\ & + A_y^2\Omega_{yy}^2 \exp\left(-\Omega_{yy}^2k^2\rho^2/2f^2\right). \end{aligned} \tag{40}$$

These scintillation coefficients are, in contrast to their counterparts in the front focal plane, not uniform but clearly depend on the radial distance ρ. An example is shown in Fig. 1. The four scintillation coefficients display strikingly different behavior. For example, the "traditional" scintillation coefficient $D_{00}^{N(f)}$, represented by the solid blue curve, is larger at the geometrical focus ($\rho = 0$) than its twin in the front focal plane, $D_{00}^{N(\mathrm{in})}$ (dashed blue curve), namely, 0.84 vs 0.61.

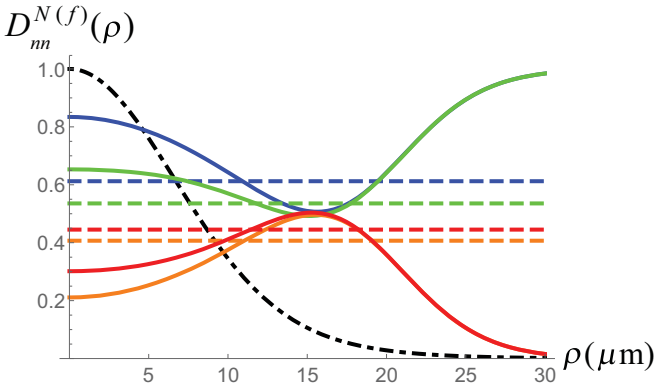

FIG. 1. The four scintillation coefficients $D_{nn}^{N(f)}(\rho)$ in the back focal plane. The upper (at the left-hand side of the plot) solid curve blue represents $D_{00}^{N(f)}(\rho)$; the upper dashed blue line is its counterpart in the front focal plane $D_{00}^{N(\mathrm{in})}$. The solid green curve (second from top) is for $D_{11}^{N(f)}(\rho)$; the dashed green line (second from top) is for $D_{11}^{N(\mathrm{in})}$. The lowest solid orange curve depicts $D_{22}^{N(f)}(\rho)$; the lowest dashed orange line shows $D_{22}^{N(\mathrm{in})}$. The third solid (red) curve from the top represents $D_{33}^{N(f)}(\rho)$, whereas the red dashed line (third from the top) represents $D_{33}^{N(\mathrm{in})}$. The dash-dotted black curve is the spectral density. In this example $f = 25$ cm, $\lambda = 632.8$ nm, $A_x = 1$, $A_y = 1.5$, $\sigma = 1$ cm, $|B_{xy}| = 0.3$, $\phi = \pi/3$, $\delta_{xx} = 2.5$ mm, $\delta_{yy} = 4.0$ mm, and $\delta_{xy} = 4.5$ mm.

The value of $D_{00}^{N(f)}$ gradually decreases to about 0.5 and then increases to unity. This is in marked contrast to, for example, $D_{33}^{N(f)}$, which is shown as the solid red curve. This coefficient at the geometrical focus is less than $D_{33}^{N(\mathrm{in})}$ (0.29 vs 0.44), and it first increases before eventually tending to zero. In Eqs. (39a) and (39b) the third term decreases much faster with increasing ρ than the first two terms. That means that when $\rho > 16\ \mu$m the curves for $D_{00}^{N(f)}$ and $D_{11}^{N(f)}$ overlap. The same applies for the second term that occurs in the expressions for $D_{22}^{N(f)}$ and $D_{33}^{N(f)}$.

It is straightforward to verify that the scintillation coefficients in the back focal plane again satisfy the sum rule given by Eq. (19), namely,

$$\sum_{n=0}^{3} D_{nn}^{N(f)}(\rho) = 2. \tag{41}$$

This sum rule opens up the intriguing possibility of what we might term, in analogy to a well-known concept in quantum optics [30], scintillation squeezing. By changing the parameters of the incident beam, the scintillation of one particular Stokes parameter of the focused field can be decreased while changing those of the others. In this process their total sum remains fixed at 2. It should be noted that, under the assumption of Gaussian statistics, the traditional scintillation coefficient $D_{00}^{N(f)}$ is bounded, namely [24],

$$\tfrac{1}{2} \leqslant D_{00}^{N(f)} \leqslant 1, \tag{42}$$

which obviously limits scintillation squeezing.

Table I illustrates the process of squeezing. The four Stokes scintillations at the geometrical focus are shown for various values of $|B_{xy}|$, the modulus of the correlation coefficient that

TABLE I. Scintillation squeezing. In this example the parameters are taken as $A_x = A_y = 1$, $\lambda = 632.8$ nm, $\sigma = 5$ mm, $\phi = \pi/3$, $\delta_{xx} = 3.0$ mm, $\delta_{yy} = 3.5$ mm, and $\delta_{xy} = 5.0$ mm.

Scintillation at focus	$\lvert B_{xy}\rvert = 0.41$	$\lvert B_{xy}\rvert = 0.2$	$\lvert B_{xy}\rvert = 0$
$D_{00}^{N(f)}$	0.88	0.60	0.51
$D_{11}^{N(f)}$	0.14	0.42	0.51
$D_{22}^{N(f)}$	0.31	0.45	0.49
$D_{33}^{N(f)}$	0.67	0.53	0.49
sum	2	2	2

was defined in Eq. (23). In the table this modulus ranges from zero to the upper bound given by Eq. (29). It is seen that $D_{00}^{N(f)}$ can be lowered significantly by decreasing $|B_{xy}|$. However, this leads to an increase of the second coefficient $D_{11}^{N(f)}$. A similar trade-off occurs for the other two Stokes scintillation coefficients. Changing $|B_{xy}|$ is of course just one way to squeeze the Stokes scintillations. Another example is presented in Table II, where the on-axis scintillations are shown for selected values of the coherence radius δ_{xx}. It is seen that whereas $D_{11}^{N(f)}$ can be changed substantially, this is not the case for $D_{22}^{N(f)}$.

By tuning the various source parameters, one can design a focused field in which the fluctuations of a prescribed Stokes parameter are minimized. For example, partially coherent light is sometimes used to reduce unwanted speckle (see [31]). If such light is focused onto a chiral object that is particularly sensitive to one type of circular polarization, it may be advantageous to minimize the scintillation of S_3.

Whereas the examples of the diagonal Stokes scintillations $D_{nn}^{N(f)}(\boldsymbol{\rho})$ that we discussed so far are all positive valued, this is not always the case for the off-diagonal scintillations. For example, from Eq. (11) we find, on setting $\mathbf{r}_1 = \mathbf{r}_2$ and using Eq. (35), that

$$D_{23}^{N(f)}(\rho) = 2A_x^2A_y^2\Omega_{xy}^4|B_{xy}|^2\sin(2\phi) \times \exp\left(-\Omega_{xy}^2k^2\rho^2/f^2\right)/\Lambda^2(\rho). \tag{43}$$

Clearly, this coefficient is negative whenever $\sin(2\phi) < 0$.

TABLE II. Scintillation squeezing. The parameters are taken as $A_x = A_y = 1$, $|B_{xy}| = 0.5$, $\lambda = 632.8$ nm, $\sigma = 5$ mm, $\phi = \pi/3$, $\delta_{yy} = 3.5$ mm, and $\delta_{xy} = 5.0$ mm.

Scintillation at focus	$\delta_{xx} = 4$ mm	$\delta_{xx} = 5$ mm	$\delta_{xx} = 6$ mm
$D_{00}^{N(f)}$	0.83	0.75	0.73
$D_{11}^{N(f)}$	0.18	0.33	0.44
$D_{22}^{N(f)}$	0.33	0.35	0.34
$D_{33}^{N(f)}$	0.66	0.56	0.48
sum	2	2	2

V. STOKES FLUCTUATION CORRELATIONS

In order to study the Hanbury Brown–Twiss effect in its generalized form, we use Eqs. (6) and (15). We restrict ourselves to the four diagonal correlations. Taking the first reference point to be on the z axis ($\boldsymbol{\rho}_1 = \mathbf{0}$) and setting $\sigma_x = \sigma_y = \sigma$, we find from Eq. (23) for the HBT coefficients in the front focal plane the expressions

$$C_{00}^{N(\mathrm{in})}(0,\rho_2) = \left[A_x^4\exp\left(-\rho_2^2/\delta_{xx}^2\right) + A_y^4\exp\left(-\rho_2^2/\delta_{yy}^2\right) + 2A_x^2A_y^2|B_{xy}|^2\exp\left(-\rho_2^2/\delta_{xy}^2\right)\right]/\left(A_x^2+A_y^2\right)^2, \tag{44a}$$

$$C_{11}^{N(\mathrm{in})}(0,\rho_2) = \left[A_x^4\exp\left(-\rho_2^2/\delta_{xx}^2\right) + A_y^4\exp\left(-\rho_2^2/\delta_{yy}^2\right) - 2A_x^2A_y^2|B_{xy}|^2\exp\left(-\rho_2^2/\delta_{xy}^2\right)\right]/\left(A_x^2+A_y^2\right)^2, \tag{44b}$$

$$C_{22}^{N(\mathrm{in})}(0,\rho_2) = 2A_x^2A_y^2\left\{\exp\left[-\frac{\rho_2^2}{2}\left(\frac{1}{\delta_{xx}^2}+\frac{1}{\delta_{yy}^2}\right)\right] + |B_{xy}|^2\cos(2\phi) \times \exp\left(-\frac{\rho_2^2}{\delta_{xy}^2}\right)\right\}\Big/\left(A_x^2+A_y^2\right)^2, \tag{44c}$$

$$C_{33}^{N(\mathrm{in})}(0,\rho_2) = 2A_x^2A_y^2\left\{\exp\left[-\frac{\rho_2^2}{2}\left(\frac{1}{\delta_{xx}^2}+\frac{1}{\delta_{yy}^2}\right)\right] - |B_{xy}|^2\cos(2\phi) \times \exp\left(-\frac{\rho_2^2}{\delta_{xy}^2}\right)\right\}\Big/\left(A_x^2+A_y^2\right)^2. \tag{44d}$$

The Stokes fluctuation correlations in the front focal plane are shown in Fig. 2 for the same values of the parameters as in Fig. 1. The first of these coefficients, $C_{00}^{N(\mathrm{in})}(0,\rho_2)$, represented by the blue curve, is the traditional Hanbury Brown–Twiss coefficient. That is, it describes the correlation of the intensity

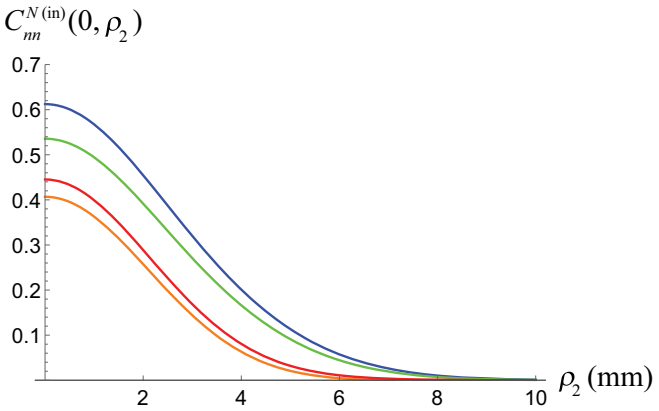

FIG. 2. The four diagonal Stokes fluctuation correlations $C_{nn}^{N(\mathrm{in})}(0,\rho_2)$ in the front focal plane. The blue (top) curve represents $C_{00}^{N(\mathrm{in})}(0,\rho_2)$, the green curve (second from top) shows $C_{11}^{N(\mathrm{in})}(0,\rho_2)$, the orange (bottom) curve is for $C_{22}^{N(\mathrm{in})}(0,\rho_2)$, and the red curve (third from top) is for $C_{33}^{N(\mathrm{in})}(0,\rho_2)$. The parameters are the same as in Fig. 1. Notice that the horizontal scale is now in millimeters rather than in microns.

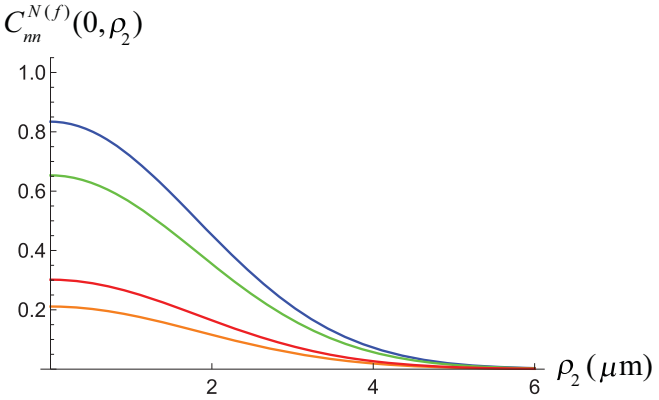

FIG. 3. The four Stokes fluctuation correlations $C_{nn}^{N(f)}(0,\rho_2)$ in the back focal plane of the lens. The blue (top) curve represents $C_{00}^{N(f)}(0,\rho_2)$, the green (second) curve is for $C_{11}^{N(f)}(0,\rho_2)$, the orange (bottom) curve shows $C_{22}^{N(f)}(0,\rho_2)$, and the red curve (third from the top) is for $C_{33}^{N(f)}(0,\rho_2)$. The parameters are the same as in Fig. 1.

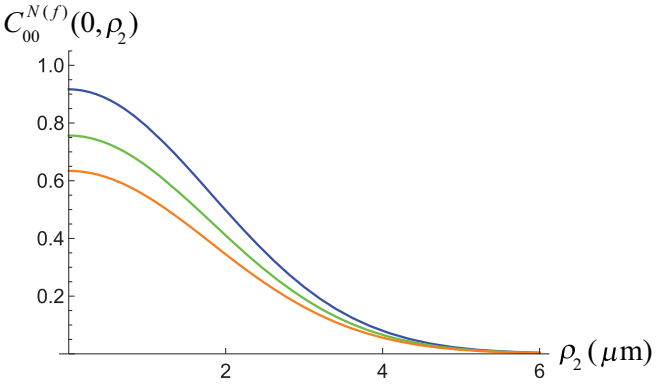

FIG. 4. Classical HBT correlation $C_{00}^{N(f)}(0,\rho_2)$ in the back focal plane for selected values of the coherence radius δ_{xx}. The curves, from top to bottom, represent the case $\delta_{xx}=2$ mm (blue), $\delta_{xx}=3$ mm (green), and $\delta_{xx}=4$ mm (orange). The other parameters are the same as in Fig. 1.

fluctuations in the front focal plane between the central axis and a point at a radial distance ρ_2.

In order to see the effect of focusing on these correlations we substitute from Eq. (35) into Eqs. (6) and (15) and again set $\boldsymbol{\rho}_1=\mathbf{0}$. This gives us, for the Stokes fluctuation correlations in the back focal plane, the four expressions

$$C_{00}^{N(f)}(0,\rho_2)=\big[A_x^4\Omega_{xx}^4\exp\big(-2\beta_{xx}\rho_2^2\big)+A_y^4\Omega_{yy}^4\times\exp\big(-2\beta_{yy}\rho_2^2\big)+2A_x^2A_y^2\Omega_{xy}^4|B_{xy}|^2\times\exp\big(-2\beta_{xy}\rho_2^2\big)\big]\big/\Lambda(0)\Lambda(\rho_2),\tag{45a}$$

$$C_{11}^{N(f)}(0,\rho_2)=\big[A_x^4\Omega_{xx}^4\exp\big(-2\beta_{xx}\rho_2^2\big)+A_y^4\Omega_{yy}^4\times\exp\big(-2\beta_{yy}\rho_2^2\big)-2A_x^2A_y^2\Omega_{xy}^4|B_{xy}|^2\times\exp\big(-2\beta_{xy}\rho_2^2\big)\big]\big/\Lambda(0)\Lambda(\rho_2),\tag{45b}$$

$$C_{22}^{N(f)}(0,\rho_2)=2A_x^2A_y^2\big\{\Omega_{xx}^2\Omega_{yy}^2\exp\big[-\big(\beta_{xx}+\beta_{yy}\big)\rho_2^2\big]+\Omega_{xy}^4|B_{xy}|^2\cos(2\phi)\times\exp\big(-2\beta_{xy}\rho_2^2\big)\big\}\big/\Lambda(0)\Lambda(\rho_2),\tag{45c}$$

$$C_{33}^{N(f)}(0,\rho_2)=2A_x^2A_y^2\big\{\Omega_{xx}^2\Omega_{yy}^2\exp\big[-\big(\beta_{xx}+\beta_{yy}\big)\rho_2^2\big]-\Omega_{xy}^4|B_{xy}|^2\cos(2\phi)\times\exp\big(-2\beta_{xy}\rho_2^2\big)\big\}\big/\Lambda(0)\Lambda(\rho_2),\tag{45d}$$

where

$$\beta_{ij}\equiv\frac{k^2}{f^2}\left(\frac{\sigma^2}{2}+\frac{\Omega_{ij}^2}{8}\right),\tag{46}$$

with the function $\Lambda(\rho)$ defined above in Eq. (40). We note that, unlike the correlations of the incident field given by Eqs. (44a)–(44d), the correlations in the focal plane depend on the effective source width σ via the parameter β_{ij}. The first coefficient $C_{00}^{N(f)}(0,\rho_2)$ represents the usual Hanbury Brown–Twiss coefficient in the focal plane. All four correlations are illustrated in Fig. 3. In this example the HBT correlations are seen to drop off significantly faster than the Stokes scintillations that are plotted in Fig. 1.

On comparing Figs. 2 and 3 it is seen that whereas the width of the different correlations in the front focal plane is on the order of millimeters, in the back focal plane it is on the order of microns. That the action of the lens dramatically shortens the effective correlation widths is of course to be expected. However, quite surprising is the effect on the maximum value of the correlations that occurs on the z axis near $\rho_2=0$. Whereas the first two correlations $C_{00}^{N(f)}$ and $C_{11}^{N(f)}$ are stronger after the focusing process, the opposite is true for $C_{22}^{N(f)}$ and $C_{33}^{N(f)}$. These are both weaker than their counterparts in the front focal plane. This unexpected effect is due to the fact that each cross-spectral density matrix element is affected differently by the lens, as can be seen from Eq. (21). The four HBT correlations, which are combinations of these elements, are therefore all transformed differently by the focusing.

The traditional HBT correlation in the focal plane $C_{00}^{N(f)}$ depends in a complicated way on the different source parameters, as can be seen from Eq. (45a). This dependence is illustrated in Fig. 4, where the normalized correlation coefficient is plotted for several choices of the coherence radius δ_{xx}. It is seen that the correlation of the intensity fluctuations decreases when this radius is increased.

Just like the generalized scintillations that were discussed in Sec. IV, the diagonal Stokes fluctuation correlations also satisfy a sum rule, namely, Eq. (17). According to this equation, the sum of the correlations is equal to two times the modulus of $\eta(\mathbf{r}_1,\mathbf{r}_2)$, the spectral degree of coherence. It is clear from the definition of this quantity that it is described only by the diagonal elements of the cross-spectral density matrix $\mathbf{W}(\mathbf{r}_1,\mathbf{r}_2)$. Therefore, it is independent of the coefficient B_{xy} and the correlation radius δ_{xy} that are defined in Eq. (23). However, the diagonal Stokes fluctuation correlations $C_{nn}^{N(f)}(0,\rho_2)$ do depend on these two parameters, as is clear from Eqs. (45a)–(45d). This means that the strength of the four correlations can be "distributed" by varying B_{xy} or δ_{xy} while keeping their total sum fixed. This is illustrated in Table III. We find that the traditional HBT coefficient $C_{00}^{N(f)}$ can be significantly increased by varying $|B_{xy}|$ from zero to its

TABLE III. Distributing correlations: the four diagonal Stokes fluctuation correlations $C_{nn}^{N(f)}(0, \rho_2)$ in the focal plane at $\rho_2 = 2\ \mu$m. The parameters are taken as $A_x = A_y = 1$, $\sigma = 1$ cm, $f = 50$ cm, $\lambda = 632.8$ nm, $\phi = \pi/3$, $\delta_{xx} = \delta_{yy} = 2.5$ mm, and $\delta_{xy} = 3.0$ mm. In this example $|\eta(0, \rho_2)| = 0.925$.

Correlations in the focal plane	$\lvert B_{xy}\rvert = 0.00$	$\lvert B_{xy}\rvert = 0.40$	$\lvert B_{xy}\rvert = 0.69$
$C_{00}^{N(f)}$	0.43	0.57	0.84
$C_{11}^{N(f)}$	0.43	0.29	0.01
$C_{22}^{N(f)}$	0.43	0.36	0.22
$C_{33}^{N(f)}$	0.43	0.49	0.64
sum	1.71	1.71	1.71

maximum value. This is accompanied by a strong decrease to almost zero of $C_{11}^{N(f)}$.

VI. CONCLUSION

We have applied the recently developed framework of generalized Stokes fluctuation correlations and Stokes scintillations to the case of a focused, random electromagnetic beam. The scintillations in the back focal plane of the lens are found to be typically nonuniform. Since they satisfy a sum rule, one particular Stokes scintillation may be suppressed at the expense of others. Depending on the intended application, the source design can be optimized to make use of this effect.

The generalized Hanbury Brown–Twiss correlations are also strongly influenced by the focusing process. Their maximum value can be either lower or higher than that of the same correlation in the front focal plane. Just like the generalized scintillations, the generalized correlations are also related by a sum rule. This gives the possibility for a trade-off between their relative strengths.

Our analysis shows that the state of coherence of the incident field significantly affects the generalized HBT correlations and the scintillation of the four Stokes parameters. We illustrated our results for the case of a Gaussian Schell-model beam. It will be useful to extend the analysis to other types of beams such as vortex beams or Bessel-correlated beams.

ACKNOWLEDGMENTS

This work was supported by the Air Force Office of Scientific Research under Award No. FA9550-16-1-0119. Y. W. is supported by the Excellent Doctorate Foundation of Northwestern Polytechnical University.

[1] R. Hanbury Brown and R. Q. Twiss, A new type of interferometer for use in radio astronomy, Philos. Mag. **45**, 663 (1954).
[2] R. Hanbury Brown and R. Q. Twiss, Correlation between photons in two coherent beams of light, Nature (London) **177**, 27 (1956).
[3] R. Hanbury Brown, *The Intensity Interferometer* (Taylor & Francis, London, 1974).
[4] G. Baym, The physics of Hanbury Brown–Twiss intensity interferometry: From stars to nuclear collisions, Acta Phys. Pol. B **29**, 1839 (1998).
[5] A. Öttl, S. Ritter, M. Köhl, and T. Esslinger, Correlations and Counting Statistics of an Atom Laser, Phys. Rev. Lett. **95**, 090404 (2005).
[6] M. Schellekens, R. Hoppeler, A. Perrin, J. Viana Gomes, D. Boiron, A. Aspect, and C. I. Westbrook, Hanbury Brown–Twiss effect for ultracold quantum gases, Science **310**, 648 (2005).
[7] T. Jeltes, J. M. McNamara, W. Hogervorst, W. Vassen, V. Krachmalnicoff, M. Schellekens, A. Perrin, H. Chang, D. Boiron, A. Aspect, and C. I. Westbrook, Comparison of the Hanbury Brown–Twiss effect for bosons and fermions, Nature (London) **445**, 402 (2007).
[8] D. Kuebel, T. D. Visser, and E. Wolf, Application of the Hanbury Brown–Twiss effect to scattering from quasi-homogeneous media, Opt. Commun. **294**, 43 (2013).
[9] G. Wu and T. D. Visser, Correlation of intensity fluctuations in beams generated by quasi-homogeneous sources, J. Opt. Soc. Am. A **31**, 2152 (2014).
[10] R. Liu, F. Wang, D. Chen, Y. Wang, Y. Zhou, H. Gao, P. Zhang, and F. Li, Measuring mode indices of a partially coherent vortex beam with Hanbury Brown and Twiss type experiment, Appl. Phys. Lett. **108**, 051107 (2016).
[11] T. Shirai, in *Progress in Optics*, edited by T. D. Visser (Elsevier, Amsterdam, 2017), Vol. 62, pp. 1–72.
[12] T. Hassinen, J. Tervo, T. Setälä, and A. T. Friberg, Hanbury Brown–Twiss effect with electromagnetic waves, Opt. Express **19**, 15188 (2011).
[13] X. Liu, G. F. Wu, X. Pang, D. Kuebel, and T. D. Visser, Polarization and coherence in the Hanbury Brown–Twiss effect, J. Mod. Opt. **65**, 1437 (2018).
[14] D. Kuebel and T. D. Visser, Generalized Hanbury Brown–Twiss effect for Stokes parameters, J. Opt. Soc. Am. A **36**, 362 (2019).
[15] G. F. Wu, D. Kuebel, and T. D. Visser, Generalized Hanbury Brown–Twiss effect in partially coherent electromagnetic beams, Phys. Rev. A **99**, 033846 (2019).
[16] J. J. Stamnes, *Waves in Focal Regions* (Hilger, Bristol, 1986).
[17] T. D. Visser, G. Gbur, and E. Wolf, Effect of the state of coherence on the three-dimensional spectral intensity distribution near focus, Opt. Commun. **213**, 13 (2002).
[18] S. B. Raghunathan, T. van Dijk, E. J. G. Peterman, and T. D. Visser, Experimental demonstration of an intensity minimum at the focus of a laser beam created by spatial coherence: Application to optical trapping of dielectric particles, Opt. Lett. **35**, 4166 (2010).
[19] D. G. Fischer and T. D. Visser, Spatial correlation properties of focused partially coherent light, J. Opt. Soc. Am. A **21**, 2097 (2004).
[20] T. D. Visser, G. P. Agrawal, and P. W. Milonni, Fourier processing with partially coherent fields, Opt. Lett. **42**, 4600 (2017).
[21] X. Zhao, T. D. Visser, and G. P. Agrawal, Degree of polarization in the focal region of a lens, J. Opt. Soc. Am. A **35**, 1518 (2018).

[22] E. Wolf, *Introduction to the Theory of Coherence and Polarization of Light* (Cambridge University Press, Cambridge, 2007).

[23] L. C. Andrews and R. L. Phillips, *Laser Beam Propagation through Random Media*, 2nd ed. (SPIE, Bellingham, 2005).

[24] A. T. Friberg and T. D. Visser, Scintillation of electromagnetic beams generated by quasi-homogeneous sources, Opt. Commun. **335**, 82 (2015).

[25] R. M. A. Azzam, Stokes-vector and Mueller-matrix polarimetry, J. Opt. Soc. Am. A **33**, 1396 (2016).

[26] J. W. Goodman, *Introduction to Fourier Optics*, 2nd ed. (McGraw-Hill, New York, 1996), Sec. 5.2.

[27] X. Zhao, T. D. Visser, and G. P. Agrawal, Controlling the degree of polarization of partially coherent electromagnetic beams, Opt. Lett. **43**, 2344 (2018).

[28] F. Gori, M. Santarsiero, R. Borghi, and V. Ramírez-Sánchez, Realizability condition for electromagnetic Schell-model sources, J. Opt. Soc. Am. A **25**, 1016 (2008).

[29] O. Korotkova, M. Salem, and E. Wolf, Beam conditions for radiation generated by an electromagnetic Gaussian Schell-model source, Opt. Lett. **29**, 1173 (2004).

[30] R. Loudon, *The Quantum Theory of Light*, 3rd ed. (Oxford University Press, Oxford, 2000).

[31] L. Mandel and E. Wolf, *Optical Coherence and Quantum Optics* (Cambridge University Press, Cambridge, 1995), p. 260.